Volume 148
Number 9
7 May 2023
Pages 1901-2190

Analyst

rsc.li/analyst

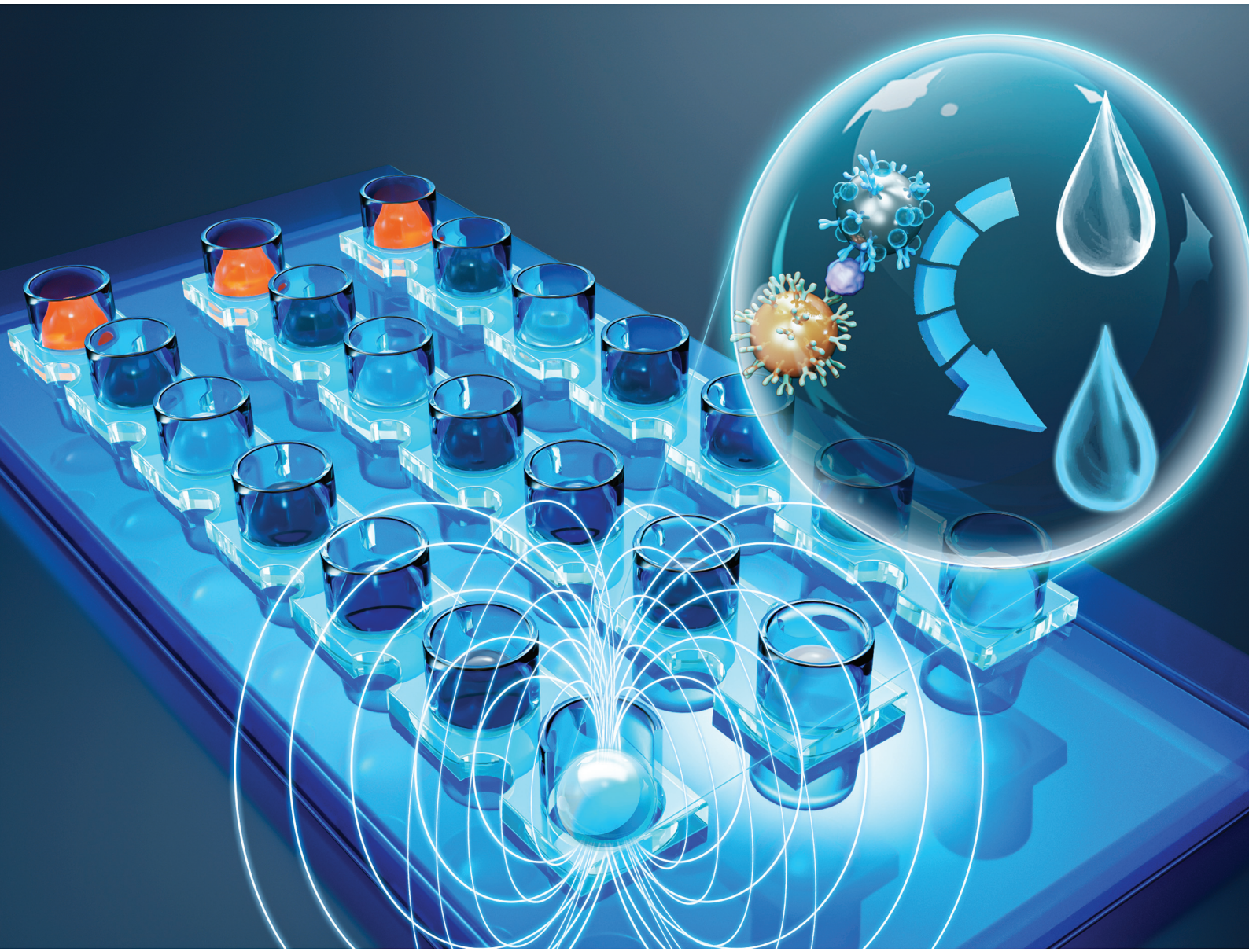

ISSN 0003-2654

ROYAL SOCIETY OF CHEMISTRY

PAPER

Shilun Feng, Bei Li *et al.*

A microfluidic immunosensor for automatic detection of carcinoembryonic antigen based on immunomagnetic separation and droplet arrays

Analyst

ROYAL SOCIETY OF CHEMISTRY

PAPER

View Article Online
View Journal | View Issue

Check for updates

Cite this: *Analyst*, 2023, **148**, 1939

A microfluidic immunosensor for automatic detection of carcinoembryonic antigen based on immunomagnetic separation and droplet arrays†

Haoran Hu, ‡[a,b,c] Gaozhe Cai,‡[b] Zehang Gao, [b,d] Cheng Liang,[e] Fengna Yang,[a,c] Xiaohui Dou,[a,c] Chunping Jia,[b] Jianlong Zhao,[b] Shilun Feng*[b] and Bei Li*[a,c]

Received 24th November 2022,
Accepted 14th February 2023

DOI: 10.1039/d2an01922a

rsc.li/analyst

Diagnosis of cancer by biomarkers plays an important role in human health and life. However, current laboratory techniques for detecting cancer biomarkers still require laborious and time-consuming operation by skilled operators and associated laboratory instruments. This work presents a colorimetric biosensor for the rapid and sensitive detection of carcinoembryonic antigen (CEA) based on an automated immunomagnetic separation platform and a droplet array microfluidic chip with the aid of an image analysis system. Immunomagnetic nanoparticles (MNPs) were used to capture CEA in the samples. CEA-detecting antibodies and horseradish peroxidase (HRP) were modified on polystyrene microspheres (PS), catalysing hydrogen peroxide and 3,3′,5,5′-tetramethylbenzidine (TMB) as signal outputs. Color reaction data were analyzed to establish a CEA concentration standard curve. The movement of MNPs between droplets in the microfluidic chip is achieved using an automatically programmable magnetic control system. This colorimetric biosensor has been used for the simultaneous detection of six CEA samples ranging from 100 pg mL^{-1} to 100 ng mL^{-1} with a detection limit of 14.347 pg mL^{-1} in 10 min, following the linear equation: $y = -4.773 \ln(x) + 156.26$ with a correlation of $R^2 = 0.9924$, and the entire workflow can be completed within 80 minutes. The microfluidic immunosensor designed in this paper has the advantages of low cost, automation, low sample consumption, high throughput, and promising applications in biochemistry.

1. Introduction

In recent years, more and more people are concerned about cancer because of the high incidence and mortality rate. Cancer is a serious threat to human health and life, ranking second in the list of causes of death, after cardiovascular disease in 2020; cancer causes nearly 10 million deaths.[1] Early diagnosis, intervention and curative effect monitoring of cancer are necessary to improve patient survival and significantly reduce patient suffering. Studies have shown that the occurrence of malignant tumours is closely related to the changes in the gene expression of related proteins in cells.[2] Therefore, a rapid, accurate, and sensitive method for detecting cancer cells and their gene expression levels is significant for cancer pathogenesis research, early diagnosis, treatment, and disease monitoring. Among them, the detection of cancer-related protein markers has become one of the most widely used clinical and laboratory detection methods.[3]

A large amount of clinical data shows that carcinoembryonic antigen (CEA), as a broad-spectrum cancer marker, has important clinical value in the differential diagnosis, disease monitoring, and efficacy evaluation of cancers such as gastric cancer, lung cancer, and colorectal cancer.[4] Current CEA detection methods mainly include enzyme-linked immunosorbent assay (ELISA),[5,6] electrochemistry,[7,8] surface plasmon resonance,[9,10] biosensors,[11,12] and fluorescence immunoassay.[13,14] Among all these methods, biosensors have been widely researched and developed as a tool in the medical, environmental, food, and pharmaceutical fields. Easy, rapid, low-cost, highly sensitive and highly selective biosensors contribute to advances in next generation pharmaceutical techno-

[a]*School of Ophthalmology & Optometry, Eye Hospital, Wenzhou Medical University, Wenzhou, 325027, China. E-mail: beili@ciomp.ac.cn*
[b]*State Key Laboratory of Transducer Technology, Shanghai Institute of Microsystem and Information Technology, Chinese Academy of Sciences, Shanghai 200050, China. E-mail: shilun.feng@mail.sim.ac.cn*
[c]*State Key Laboratory of Applied Optics, Changchun Institute of Optics, Fine Mechanics and Physics, Chinese Academy of Sciences, Changchun, 130033, PR China*
[d]*Department of Clinical Laboratory, Third Affiliated Hospital of Guangzhou Medical University, Guangdong 510150, China*
[e]*State Key Laboratory of Marine Resources Utilization in South China Sea and Center for Eco-Environment Restoration of Hainan Province, Hainan University, Haikou 570228, China*

†Electronic supplementary information (ESI) available. See DOI: https://doi.org/10.1039/d2an01922a

‡The authors contributed equally to this work.

logies such as individualized medicine and ultra-sensitive point-of-care detection of biomarkers for different diseases. Feng *et al.* developed an enzyme immunoassay (EIA) chip using an electrochemical biosensor for prostate-specific antigen (PSA) detection.[15] Wang *et al.* developed an ELISA biosensor to measure CD4+ T lymphocyte counts using an automated micro-a-fluidic platform.[16] Xu *et al.* found a new ultrasensitive sandwich-type immunoassay biosensor to detect the CEA concentration with a detection limit of 0.07 pg mL^{-1} and a linear detection range from 0.1 pg mL^{-1} to 200 ng mL^{-1}.[17] However, these methods need complex sample preparation processes or bulky detection equipment, which restricts their application in resource-limited settings and point-of-care testing (POCT) away from central laboratories. In biosensing detection, microfluidic devices have recently received increasing attention. Microfluidic devices offer a new solution for biosensor assays because of their advantages such as low biological sample consumption and precise control. However, most of these microfluidic devices require supporting external instruments and are not suitable for immediate use. For example, most microfluidic devices contain complex microfluidic components such as microvalves, micropumps, and interface connections. Additionally, traditional microfluidic bioanalytical systems often require bulky and expensive peripheral accessories such as various pressure pumps and corresponding control systems that are not portable.[18]

One primary form of the microfluidic device is a droplet-array microfluidic device. Its applications range from rapid analytical systems or synthesis of advanced materials to bioassays of proteins. Precise control of the droplet volume and reliable manipulation of individual droplets such as coalescence, mixing of their contents, and classification combined with rapid analytical tools allows us to perform chemical reactions inside droplets under defined conditions.[19] Droplet-array microfluidic devices manipulate droplets on a concave surface. Such droplets function both as reaction chambers and fluid transportation units.[20] At the same time, immiscible liquids can be used to isolate samples and reagents from the environment. Many actuation methods have been developed to control the droplet movement, including passive actuation and active actuation, such as surface acoustic waves,[21–23] electrowetting,[24–26] or magnetic forces.[27–29] The magnetic-based operating method offers particular advantages because of its flexibility and ease of operation. The use of permanent magnets avoids the need for an external fluid control unit, thus significantly reducing manufacturing and operating costs.

In this paper, a microfluidic immunosensor based on an automated magnetic control system is designed to detect the CEA concentration. Enrichment of CEA in the detection sample using the immunomagnetic separation technique to improve the detection performance of the immunosensor. As shown in Fig. 1A & E, the microfluidic chip is composed of a PDMS channel layer with holes and a glass substrate layer. We developed a magnetic control system which is shown in Fig. 1B to automatically control the magnetic nanoparticles (MNPs) in the droplet. The magnetic control system mainly

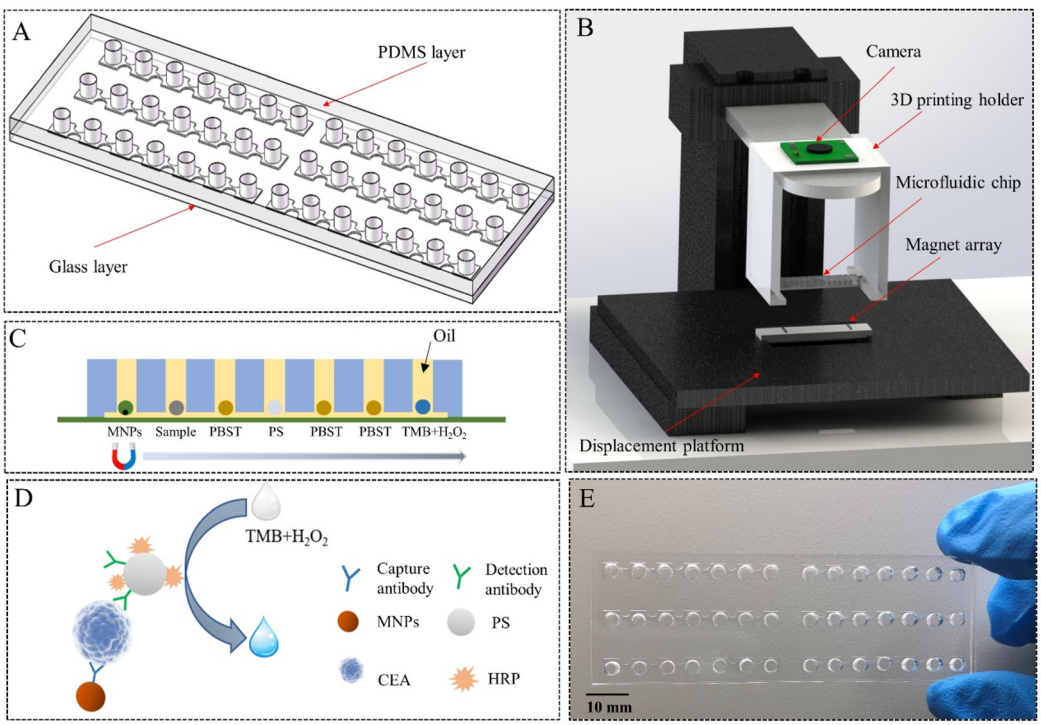

Fig. 1 Overall schematic diagram of this work. (A) A design drawing of the chip. The upper layer is a perforated PDMS channel layer and the lower layer is a glass supporting layer; (B) schematic diagram of the working system; (C) schematic diagram of liquid phase reagent filling and the section of the chip; (D) schematic diagram of the detection principle; and (E) picture of the chip used in this work.

consists of a USB camera that can be used to observe the entire automated workflow, a 3D printed holder for placing the microfluidic chip, a magnet array and a displacement platform for controlling the MNPs. The detection process of the microfluidic system is shown in Fig. 1C. Before detection, the microfluidic chip was filled with mixed mineral oil (3.6%, w/w, EM90; 0.12%, w/w, Triton X-100). The CEA capture antibody was modified on the surface of the MNPs to capture and enrich CEA in the sample. In addition, the CEA detection antibody and horseradish peroxidase (HRP) were modified on the polystyrene microspheres (PS). The MNPs were first enriched and moved to the sample droplet by the magnet array for capturing CEA, followed by washing with PBST and reacting with immune-PS to form the MNP–CEA–PS complex. Finally, the complex was moved to the droplet containing 3,3′,5,5′-tetramethylbenzidine (TMB) and hydrogen peroxide (H_2O_2). HRP on the complexes catalyzes TMB and H_2O_2, prompting a color change in the chamber filled with the reaction solution (Fig. 1D), which is used to determine the concentration of CEA in the sample. In order to improve throughput, we designed 6 detection channels on the same chip, so the chip in this paper can detect 6 samples at the same time.

2. Materials and methods

2.1 Materials and reagents

Magnetic nanoparticles were purchased from Allrunnano (Shanghai, CN). Polystyrene microspheres (PS) were purchased from Bangs Lab (Indiana, USA). The capture antibody and detection antibody were purchased from Medix Biochemica (Shanghai, CN). Carcinoembryonic antigen (CEA) was purchased from Lee Biosolutions, Inc (Maryland Heights, MO USA 63043). 3-(Ethyliminomethylideneamino)-*N* (EDC) and *N*-hydroxysulfosuccinimide (NHSS) for magnetic bead activation were purchased from Sigma-Aldrich (St Louis, MO, USA). TMB color reagent A solution (3,3′,5,5′-tetramethylbenzidine) and TMB color reagent B solution (peroxide solution) were purchased from Aladdin (Shanghai, CN). Horseradish peroxide (HRP) and Proclin 300 were purchased from Solarbio (Beijing, CN). A silicone elastomer kit for fabricating a polydimethylsiloxane (PDMS) chip was purchased from Dow Corning (Sylgard 184, Auburn, MI, US). Phosphate buffered saline (PBS), phosphate buffered (PB), Tween-20, and Triton X-100 were purchased from Sangon Biotech Co. Ltd (Shanghai, CN). EM 90 was purchased from Biohope Inc (Shanghai, CN). A Formlabs Form3 3D printer was purchased from Formlabs (Somerville, Massachusetts, USA).

2.2 Design and fabrication of the microfluidic immunosensor chip

The microfluidic immunosensor chip is the key component of this detection system. The chip consists of two layers: a PDMS top layer with microfluidic channels (thickness: 4 mm) and a glass bottom layer (thickness: 0.5 mm). A chip has six droplet microfluidic channels for CEA detection, each channel has seven square chambers (length: 3 mm and height: 150 μm) for filling with different reagents. These chambers are arranged in a straight line. The link channel between the two square chambers (width: 700 μm and height: 150 μm) is used to facilitate the passage of MNPs and to confine the reagent droplets filling the through-holes. The detailed design of the microfluidic chip can be found in Fig. S1.† The mould of the PDMS layer was fabricated by patterning a negative photoresist (SU-8 3050, Microchem, Durham Magneto Optics, UK) on a silicon wafer using a direct laser writing system (MicroWriter ML3, Durham Magneto Optics, UK). The manufacturing process of the chip is shown in Fig. S2.† Then, the PDMS prepolymer and the curing agent were mixed well in a ratio of 10 : 1, vacuumed for 10 min, and the mixture was poured on the silicon wafer mould after the air bubbles were removed and cured at 80 °C for 2 hours. After that, the PDMS layer was peeled off from the mould and punched at the middle area of the square chamber to form circle through-holes (diameter: 3 mm). Then, the glass was washed with anhydrous ethanol and bonded to the PDMS layer using oxygen plasma treatment (PDC-002, Harrick Plasma, Ithaca, NY, US). After bonding two layers, the chip was placed in a 60 °C oven to enhance the bonding effect.

2.3 Preparation of immune MNPs

A 10 mL glass bottle was soaked in chromic acid overnight and cleaned with pure water before preparation, followed by washing with 5 mL of PB (0.01 M, pH 6.0) three times. Then, 50 μL of MNPs (10 mg mL^{-1}) was added to the bottle and washed with 3 mL of PB (0.01 M, pH 6.0) three times. After washing, the MNPs were dissolved with 3 mL of PB (0.01 M, pH 6.0), followed by adding 50 μL of EDC (10 mg mL^{-1} in 0.01 M PB, pH 6.0) and 50 μL of NHSS (10 mg mL^{-1} in 0.01 M PB, pH 6.0) and activated for 1 h at room temperature (180 rpm). After that, the activated MNPs were washed with 3 mL of PB (0.01 M, pH 8.4) three times and dissolved in 3 mL of PB (0.01 M, pH 8.4), followed by adding 10 μL of capture antibody (5 mg mL^{-1}) and incubating for 2 h at room temperature (180 rpm). After antibody conjugation, 1% of skim milk solution was added into the above solution to block for 1 h at room temperature (180 rpm). Finally, the immune MNPs were washed with PBS (0.01 M, pH 7.4) three times and dissolved in 1 ml of special reconstituted solution (25% sucrose, 1% skim milk, and 0.7% Proclin), and stored at 4 °C for further use.

Electron scanning microscopy (SEM) was used to observe the MNPs without and with modification of the antibody. As shown in Fig. 2A and B, the surface of the immune MNPs changed roughly after conjugation with capture antibodies, which indicated the successful modification of the capture antibodies.

2.4 Preparation of immune PS–HRP

A 10 mL glass bottle and a magnetic stirrer were soaked in chromic acid overnight and cleaned with pure water before preparation, followed by washing with 5 mL of PB (0.01 M, pH 6.0) three times. Then, 30 μL of PS (10 mg mL^{-1}) was added to 1 mL of PB (0.01 M, pH 6.0) in a 1.5 ml centrifuge tube. After

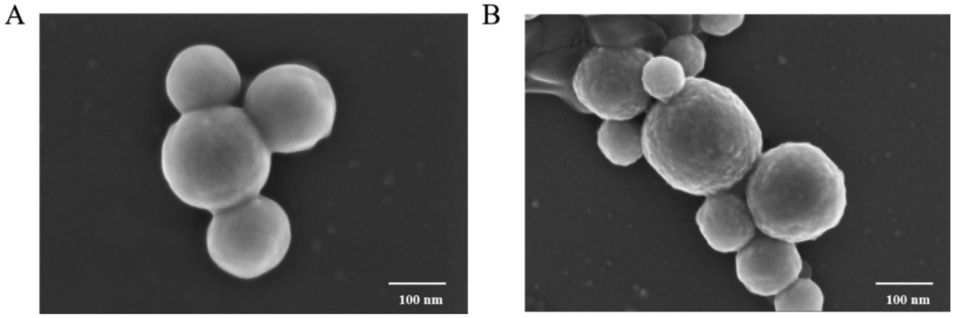

Fig. 2 (A) SEM image of pure MNPs; (B) SEM image of immune MNPs.

uniform mixing and centrifuging for 20 min (12 000 rpm, 4 °C), 1 mL of PB (0.01 M, pH 6.0) was added for resuspension. After that, 2.5 mL of PB (0.01 M, pH 6.0) and 66 μL of centrifuged PS solution were added into the glass bottle, followed by adding 5 μL of detection antibody (5 mg mL^{-1}) and 175 μL of HRP (1 mg mL^{-1} in 0.01 M PB, pH 6.0) to react for 1 h (800 rpm). Then, 30 μL of EDC (1 μg μL^{-1} in 0.01 M PB, pH 6.0) was added once an hour for a total of three times. After conjugation, 300 μL of skim milk solution (10%, 0.01 M PB, pH 6.0) and 50 μL of EDC (1 μg μL^{-1} in 0.01 M PB, pH 6.0) were added to the reaction system at room temperature and reacted for 1 h (800 rpm). Then, the reagent in the glass bottle was transferred into a centrifuge tube for centrifugation (10 000 rpm, 4 °C, 20 min) and the supernatant was removed, followed by dissolving the precipitate in 500 μL of special reconstituted solution (25% sucrose, 1% skim milk, and 0.7% Proclin). Finally, the immune PS–HRP solution was stored at 4 °C for further use.

2.5 Surface treatment of the microfluidic immunosensor chip

Since the PDMS layer and the glass layer are bonded by oxygen plasma treatment, which greatly enhances the hydrophilicity of the glass and PDMS surfaces, the bonded chip remains hydrophilic. This can easily cause the droplets to adhere to the wall and some MNPs are adsorbed on the inner wall of the chip together with the droplets, which will affect the transfer efficiency of the MNPs between two droplets and cause reagent leakage between adjacent cavities. In addition, it can adversely affect the program positioning function. Therefore, it is necessary to change the microfluidic chip to a hydrophobic state. In this paper, 110 °C is used as the treatment temperature to study the recovery of the hydrophobic state of the chip at different treatment times.

As shown in Fig. 3A, 0.05% PBST (pH 7.4) was mixed with yellow dye as the liquid phase, and it can be seen that the droplets stick to the wall and are in an irregular form when there is no high temperature baking. When treated at 110 °C for 5 minutes, it can be seen from the top view that some droplets are still adhering to the wall. When maintained at 110 °C for 10 minutes of treatment, the droplets were essentially located in the center of the chamber, away from the walls. From the side view, it can also be noticed that each droplet shows a good droplet shape in the chip. Therefore, the microfluidic chip was pre-treated at 110 °C for 10 minutes before the experiment to ensure the accuracy of the detection.

In addition, a washing efficiency experiment was performed to determine the number of appropriate washing chambers. 0.05% PBST (pH 7.4) with blue dye was used to remelt the MNPs and it was filled into the chip. Then, a magnet was used to move the MNPs. As shown in Fig. 3B, after moving the MNPs to the fourth chamber, there was little blue dye left in the droplet of the third chamber. By analyzing the collected image data, we obtained the gray value of each chamber and the relationship between the blue dye left in the chamber and the gray value is shown in Fig. 3C. After washing twice, about 93.3% blue dye was washed out. Therefore, we set up two chambers in front of the color reaction chamber for filling with washing reagent droplets.

3. Results and discussion

3.1 The workflow of the immunosensor

The workflow of this proposed immunosensor is shown in Fig. 4. Prior to the detection, a mixed mineral oil is pre-filled into the chip to isolate the droplets from the environment. In the first chamber, we injected 10 μL of mixed mineral oil and the remaining chambers were filled with 8 μL of mineral oil. Next, we filled the chambers with reagents, each chamber is filled with 5 μL of the corresponding reagents. Then, the chip is placed into the system for detection. First, the MNPs are enriched and moved to the second chamber to capture the CEA in the sample droplet and form an MNP–CEA complex. Then, the MNP–CEA complex is moved to the fourth chamber to react with immunized PS–HRP to form MNP–CEA–PS–HRP complexes through a washing chamber which is filled with 0.05% PBST (pH = 7.4). Finally, the complex is moved to the last chamber after two washing chambers. The HRP on the complex could catalyse a mixture of TMB and H_2O_2 in the chamber to induce a color change, which could be referred to as the concentration of CEA. By taking the picture of the last chamber using a USB camera and processing the collected image data, the standard curve of the color index and the CEA concentration could be established. The detection procedure can be completed within

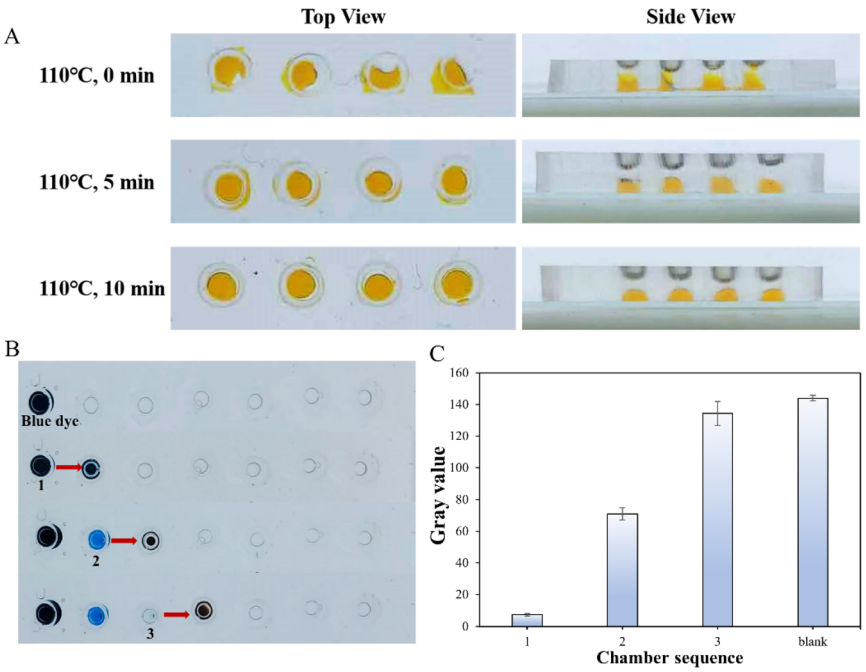

Fig. 3 (A) Top and side views of the droplet morphology in the chip after 110 °C treatment at 0 minutes, 5 minutes and 10 minutes; (B) 0.05% PBST with blue dye remelted MNP washing test; (C) the relationship between the blue dye left in the droplet of different chambers and the gray value and error bars show the standard deviations of measurements from at least three separate experiments.

Fig. 4 Schematic diagram of CEA detection workflow. (a) Using a magnet to enrich MNPs; (b) MNPs capture CEA in the sample; (c) 0.05% PBST (pH 7.4) wash MNPs and CEA; (d) MNPs and CEA bond PS–HRP; (e) 0.05% PBST (pH 7.4) first wash MNPs, CEA and PS–HRP; (f) 0.05% PBST (pH 7.4) second wash MNPs, CEA and PS-HRP; and (g) color reaction of the TMB mixed solution catalyzed by HRP.

80 minutes. Besides, the workflow of the system taken using the USB camera is shown in ESI Video S1.†

3.2 Optimization of the microfluidic immunosensor chip

After the MNPs move to the next chamber, the transfer efficiency of the MNPs between two chambers is an important parameter in this work. The magnet moving speed, the width of the link channel and the surface tension between the oil phase and the liquid phase directly affect the amounts of beads left in the droplet in the previous chamber after movement. We compared the transfer efficiency of MNPs under these different conditions. The average gray value of the MNP droplet image was used to compare the transfer efficiency. The image of the previous droplet after the magnetic movement was taken using a camera and analysed by ImageJ software. After analyzing the gray value of the detected area of the image, information on the concentration of MNPs can be derived from the results. The lower the gray value, the less MNPs remain in the previous droplet after transfer. As shown in Fig. 5A, the linear relationship between the gray value and the concentration of MNPs is confirmed and it can be expressed as y (gray value) = $-0.098x$ (concentration) + 157.72 (R^2 = 0.9885).

As shown in Fig. 5B, the gray value of the previous droplet decreased with the magnet moving speed increases, which means that a lower transfer efficiency of the MNPs was obtained with an increase in the magnet moving speed. It can be explained that when the magnet moving speed was too fast, the MNPs have no enough time to form aggregates for separating from the droplet. Besides, when the magnet speed was lower than 500 μm s^{-1}, there was no obvious difference in the gray values. Considering the time-consuming automation work, 500 μm s^{-1} was chose as the optimal speed of the magnet. The optimization of the width of the link channel was also performed. As shown in Fig. 5C, an increase in the channel width from 200 to 700 μm resulted in a higher gray value. However, when the width remains increasing to 1200 μm, the gray value of the droplet decreased. It was believed that a narrow width such as 200 μm or 500 μm will hinder the movement trend of MNPs and decrease the transfer efficiency of MNPs. In addition, a large channel width such as 1000 μm or 1200 μm will decrease the transfer efficiency of MNPs and increase the risk of reagent leakage in the chamber. Therefore, 700 μm was selected as the optimal width of the link channel. The surface tension between the oil phase and the liquid phase also affects the transfer of the MNPs between two droplets. 3.6% EM 90 and 0.12% Triton X-100 were added into mineral oil to change the surface tension of the oil–liquid phase and the transfer efficiencies of the MNPs were compared in the pure mineral oil and the mixed mineral oil. From the results in Fig. 5D, it is found that when a mixed mineral oil is used, the gray value of the transferred droplet increased a lot. The residual amount of MNPs was calculated as nearly 10% less than that of pure mineral oil. Thus, a mixed mineral oil was used in this work.

3.3 CEA detection in the microfluidic system

First, to evaluate the CEA detection performance of this microfluidic immunosensor, parallel tests on CEA with different concentrations from 100 pg mL^{-1} to 100 ng mL^{-1} in sterile

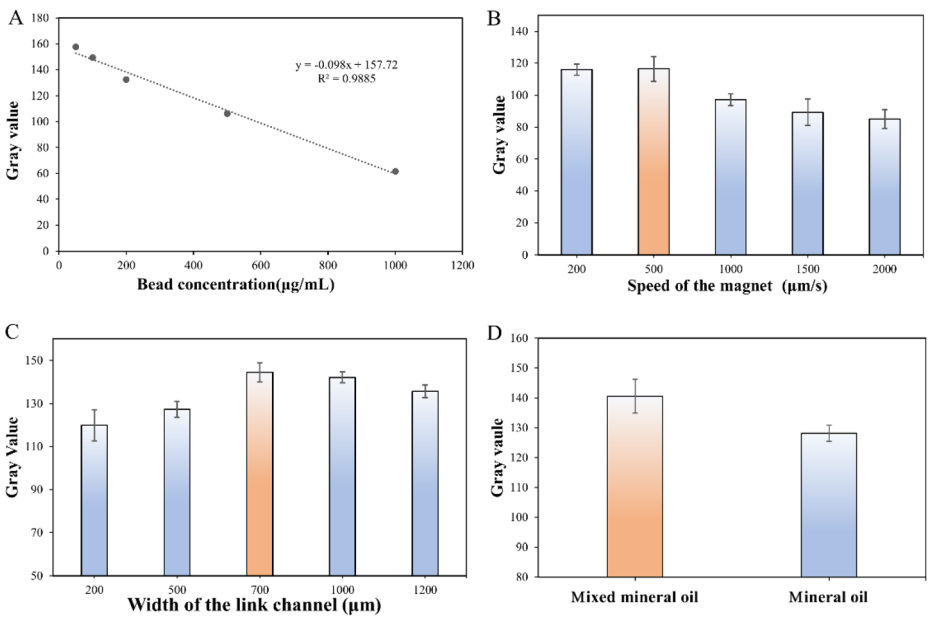

Fig. 5 Optimization data of the microfluidic immunosensor chip. Error bars show the standard deviations of measurements from at least three separate experiments. (A) Linear relationship diagram of the magnetic bead concentration and gray value, this followed a linear equation: y = $-0.098x$ + 157.72 with a correlation of R^2 = 0.9885; (B) the relationship between the speed of the magnet and the image gray value; (C) the relationship between the residual width of the link channel and the image gray value; and (D) the relationship between the different filled oil phases and the image gray value.

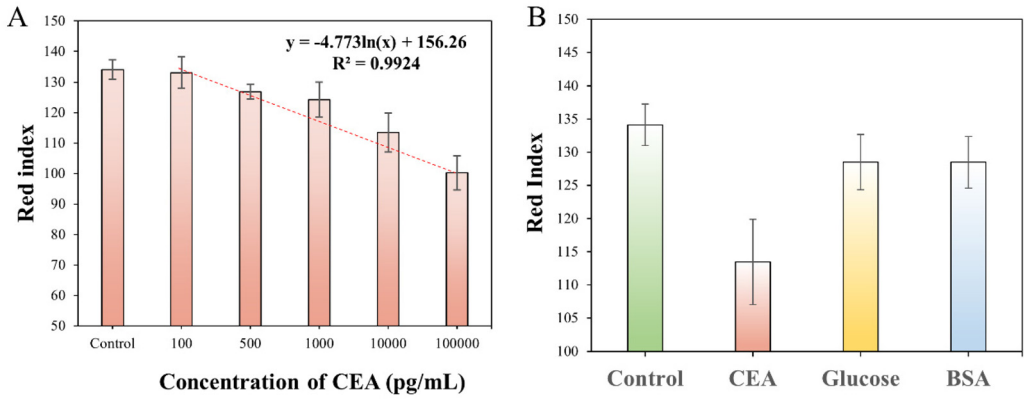

Fig. 6 Error bars show the standard deviations of measurements from at least three separate experiments. (A) The relationship between the different concentrations of CEA and the red index, this followed the linear equation: $y = -4.773\ln(x) + 156.26$ with a correlation of $R^2 = 0.9924$ and the LOD is 14.347 pg mL^{-1}; and (B) specificity comparison with the control, CEA, glucose and BSA.

Table 1 Comparison of some characteristics of this work with recently reported work of immunosensors for CEA detection

Method	Linearity range	Throughput	LOD	Time consumption	Automation	Ref.
Electrochemical	0.3–2.5 ng mL^{-1}	1 sample	10 pg mL^{-1}	20 min	NO	31
Electrochemical	0.01–10 ng mL^{-1}	1 sample	300 pg mL^{-1}	3 h	NO	32
Impedance	—	1 sample	1 ng mL^{-1}	80 min	NO	33
Lateral flow test strip	1–100 ng mL^{-1}	1 sample	45 pg mL^{-1}	—	NO	34
ELISA	0.6–7.2 ng mL^{-1}	—	156 pg mL^{-1}	—	NO	35
Droplet-array colorimetric	0.1–100 ng mL^{-1}	6 samples	14.347 pg mL^{-1}	80 min	YES	This work

PBS were conducted under optimal conditions. According to a previous work,[30] the red index of the collected image data was selected as the signal. Fig. 6A shows that the red index obtained using a camera decreased from 100.164 to 133.069 when the concentration of CEA changed from 100 pg mL^{-1} to 100 ng mL^{-1}. A linear relationship between the red index (y) and the concentration (x) was obtained and calculated as $y = -4.773\ln(x) + 156.26$ ($R^2 = 0.9924$). The detection limit of this immunosensor for CEA was calculated to be 14.347 pg mL^{-1}, which is three times that of the signal-to-noise ratio.

To investigate the specificity of this immunosensor, CEA, glucose, and BSA with the same concentration at 10 ng mL^{-1} were tested. As shown in Fig. 6B, the signal of CEA is lower than those of the control, glucose and BSA. It can be seen from the data in the figure that the immunosensor in this paper has an ideal response to CEA and good specificity for CEA detection.

Table 1 shows the CEA detecting work of other groups. The main reference detection methods are electrochemical, impedance method and MNPs. Electrochemical-based detection methods are more sensitive and have a lower LOD. However, the synthesis of electrode materials is usually more complex. The impedance-based detection method has a higher LOD. Whether based on electrochemical or impedance methods, they do not have an automated workflow. Our work has the characteristics of a lower detection limit, a large linearity range, a high throughput and automated detection.

4. Conclusion

In conclusion, this work developed a microfluidic immunosensor for the automatic detection of CEA based on immunomagnetic separation and droplet arrays. Capture antibody modified MNPs could be manipulated and transferred between different droplets with the help of an automated magneto-control system. Combining with HRP and detection antibody modified PSs, the detection of CEA with a LOD of 14.347 pg mL^{-1} in the droplet-array microfluidic chip was achieved within 80 min. This followed the linear equation: $y = -4.773\ln(x) + 156.26$, with a correlation of $R^2 = 0.9924$. Meanwhile, according to the high-throughput demand, this proposed system can detect six samples at the same time. This immunosensor exhibited high sensitivity, a wide detection range, and good selectivity and it also has the advantages of low cost, automatic operation, lower sample consumption, and a higher throughput than others. However, this proposed method for CEA detection still required 80 min from samples to results, which may affect the on-site application. Future work can be focused on shortening the detection time by replacing a two-step immunobinding reaction with a one-step immunobinding reaction, or using some other probes such as nanoantibodies or aptamers. This developed droplet-array microfluidic immunosensor system has great compatibility in the field of biological detection and broad application prospects in biochemistry by changing different probes.

Author contributions

Haoran Hu: investigation, experimental, data curation and analysis and writing the original draft. Gaozhe Cai: conceptualization, methodology, experimental guidance and review and editing. Zehang Gao: micromachining process and droplet-array microfluidic guidance. Cheng Liang: experimental and data processing assistance. Fengna Yang: data analysing assistance. Xiaohui Dou: data analysing assistance. Chunping Jia: biological experimental guidance. Shilun Feng: review and editing, supervision, and project administration. Bei Li: review and editing, and validation.

Conflicts of interest

The authors declare that they have no known competing financial interests or personal relationships that could have appeared to influence the work reported in this paper.

Acknowledgements

We would like to acknowledge the support from the equipment research and development projects of the Chinese Academy of Sciences, GJJSTD20210006 and YJKYYQ20210049. The work was also sponsored by the Shanghai Pujiang Program 21PJ1415000.

References

1 H. A.-O. Sung, J. Ferlay, R. A.-O. Siegel, M. Laversanne, I. Soerjomataram, A. Jemal and F. Bray, *Global Cancer Statistics 2020: GLOBOCAN Estimates of Incidence and Mortality Worldwide for 36 Cancers in 185 Countries*, 2020.

2 J. Yu, L. Yang and H. Lu, The emerging role of circular RNAs in common solid malignant tumors in children, *Cancer Cell Int.*, 2021, **21**, 309, DOI: **10.1186/s12935-021-01998-6**.

3 B. Zhao, J. Yan, D. Wang, Z. Ge, S. He, D. He, S. Song and C. Fan, Carbon Nanotubes Multifunctionalized by Rolling Circle Amplification and Their Application for Highly Sensitive Detection of Cancer Markers, *Small*, 2013, **9**, 2595–2601, DOI: **10.1002/smll.201202957**.

4 M. Chen, C. Zhao, Q. Xu, B. Nie, L. Xu, S. Weng and X. Lin, Electrochemical immunoassay based on polythionine as the signal source for the sensitive detection of carcinoma embryonic antigen, *Anal. Methods*, 2015, **7**, 10339–10344.

5 R. H. Gu, B. Tan, J. Ma, W. Y. Shen, Y. S. Zuo and L. Shi, Diagnostic value of the combined detection of CEA, NSE and IL-18 for lung cancer and their relationship with apoptosis gene Bcl-2, *J. Biol. Regul. Homeostatic Agents*, 2020, **34**, 1637–1646, DOI: **10.23812/20-34-a**.

6 Q. Wan, Y. Liu, B. Lv and X. Chen, Correlation of Molecular Tumor Markers CA125, HE4, and CEA with the Development and Progression of Epithelial Ovarian Cancer, *Iran. J. Public Health*, 2021, **50**, 1197–1205, DOI: **10.18502/ijph.v50i6.6418**.

7 X. Liao, X. Wang, C. Ma, L. Zhang, C. Zhao, S. Chen, K. Li, M. Zhang, L. Mei, Y. Qi, *et al.*, Enzyme-free sandwich-type electrochemical immunosensor for CEA detection based on the cooperation of an Ag/g-C(3)N(4)-modified electrode and Au@SiO(2)/Cu(2)O with core-shell structure, *Bioelectrochemistry*, 2021, **142**, 107931, DOI: **10.1016/j.bioelechem.2021.107931**.

8 W. Zhou, Y. Yang, Z. Wang, Y. Liu and M. Lari Najafi, Impact of HSP90α, CEA, NSE, SCC, and CYFRA21-1 on Lung Cancer Patients, *J. Healthcare Eng.*, 2021, **2021**, 6929971, DOI: **10.1155/2021/6929971**.

9 Z. Altintas, Y. Uludag, Y. Gurbuz and I. E. Tothill, Surface plasmon resonance based immunosensor for the detection of the cancer biomarker carcinoembryonic antigen, *Talanta*, 2011, **86**, 377–383, DOI: **10.1016/j.talanta.2011.09.031**.

10 B. Szymanska, Z. Lukaszewski, K. Hermanowicz-Szamatowicz and E. Gorodkiewicz, An immunosensor for the determination of carcinoembryonic antigen by Surface Plasmon Resonance imaging, *Anal. Biochem.*, 2020, **609**, 113964, DOI: **10.1016/j.ab.2020.113964**.

11 A. Kawamura and T. Miyata, 4.2 – Biosensors, in *Biomaterials Nanoarchitectonics*, ed. M. Ebara, William Andrew, 2016, pp. 157–176.

12 H. Muguruma, Biosensors: Enzyme Immobilization Chemistry, in *Encyclopedia of Interfacial Chemistry*, ed. K. Wandelt, Elsevier, Oxford, 2018, pp. 64–71.

13 A. Abd Temur and F. Aqeel Rashid, Irisin and Carcinoembryonic Antigen (CEA) as Potential Diagnostic Biomarkers in Gastric and Colorectal Cancers, *Rep. Biochem. Mol. Biol.*, 2021, **10**, 488–494, DOI: **10.52547/rbmb.10.3.488**.

14 L. Ding, X. Chen, L. He, F. Yu, S. Yu, J. Wang, Y. Tian, Y. Wang, Y. Wu, L. E. Liu, *et al.*, Fluorometric immunoassay for the simultaneous determination of the tumor markers carcinoembryonic antigen and cytokeratin 19 fragment using two kinds of CdSe/ZnS quantum dot nanobeads and magnetic beads, *Mikrochim. Acta*, 2020, **187**, 171, DOI: **10.1007/s00604-019-3914-7**.

15 D. Feng, J. Su, Y. Xu, G. He, C. Wang, X. Wang, T. Pan, X. Ding and X. Mi, DNA tetrahedron-mediated immune-sandwich assay for rapid and sensitive detection of PSA through a microfluidic electrochemical detection system, *Microsyst. Nanoeng.*, 2021, **7**, 33, DOI: **10.1038/s41378-021-00258-x**.

16 S. Wang, S. Tasoglu, P. Z. Chen, M. Chen, R. Akbas, S. Wach, C. I. Ozdemir, U. A. Gurkan, F. F. Giguel, D. R. Kuritzkes, *et al.*, Micro-a-fluidics ELISA for Rapid CD4 Cell Count at the Point-of-Care, *Sci. Rep.*, 2014, **4**, 3796, DOI: **10.1038/srep03796**.

17 P. Xu, W. Feng, M. Wang, L. Zhang, G. Liang and A. Jing, New Ultrasensitive Sandwich-Type Immunoassay of Dendritic Tri-Fan Blade-like PdAuCu Nanoparticles/Amine-Functionalized Graphene Oxide for Label-Free Detection of

Carcinoembryonic Antigen, *Micromachines*, 2021, **12**(10), 1256, DOI: 10.3390/mi12101256.

18 Y. Zhang, S. Park, K. Liu, J. Tsuan, S. Yang and T. H. Wang, A surface topography assisted droplet manipulation platform for biomarker detection and pathogen identification, *Lab Chip*, 2011, **11**, 398–406, DOI: 10.1039/c0lc00296h.

19 R. Seemann, M. Brinkmann, T. Pfohl and S. Herminghaus, Droplet based microfluidics, *Rep. Prog. Phys.*, 2012, **75**, 016601, DOI: 10.1088/0034-4885/75/1/016601.

20 H. Deng, A. Jayawardena, J. Chan, S. M. Tan, T. Alan and P. Kwan, An ultra-portable, self-contained point-of-care nucleic acid amplification test for diagnosis of active COVID-19 infection, *Sci. Rep.*, 2021, **11**, 15176, DOI: 10.1038/s41598-021-94652-0.

21 D. Jiang, J. Liu, Y. Pan, L. Zhuang and P. Wang, Surface acoustic wave (SAW) techniques in tissue engineering, *Cell Tissue Res.*, 2021, **386**, 215–226, DOI: 10.1007/s00441-020-03397-1.

22 T. Inui, J. Mei, C. Imashiro, Y. Kurashina, J. Friend and K. Takemura, Focused surface acoustic wave locally removes cells from culture surface, *Lab Chip*, 2021, **21**, 1299–1306, DOI: 10.1039/d0lc01293a.

23 R. Weser, A. Winkler, M. Weihnacht, S. Menzel and H. Schmidt, The complexity of surface acoustic wave fields used for microfluidic applications, *Ultrasonics*, 2020, **106**, 106160, DOI: 10.1016/j.ultras.2020.106160.

24 P. Zhao, Y. Li and H. Zappe, Accelerated electrowetting-based tunable fluidic lenses, *Opt. Express*, 2021, **29**, 15733–15746, DOI: 10.1364/oe.423460.

25 A. G. Sourais and A. G. Papathanasiou, Modelling of Electrowetting-Induced Droplet Detachment and Jumping over Topographically Micro-Structured Surfaces, *Micromachines*, 2021, **12**(6), 592, DOI: 10.3390/mi12060592.

26 I. Frozanpoor, M. D. Cooke, V. Ambukan, A. J. Gallant and C. Balocco, Continuous Droplet-Actuating Platforms via an Electric Field Gradient: Electrowetting and Liquid Dielectrophoresis, *Langmuir*, 2021, **37**, 6414–6422, DOI: 10.1021/acs.langmuir.1c00329.

27 D. Ferraro, J. Champ, B. Teste, M. Serra, L. Malaquin, S. Descroix, P. de Cremoux and J. L. Viovy, Droplet Microfluidic and Magnetic Particles Platform for Cancer Typing, *Methods Mol. Biol.*, 2017, **1547**, 113–121, DOI: 10.1007/978-1-4939-6734-6_9.

28 J. Hang, C. Hahn, N. Statuto, F. Macià and A. D. Kent, Generation and annihilation time of magnetic droplet solitons, *Sci. Rep.*, 2018, **8**, 6847, DOI: 10.1038/s41598-018-25134-z.

29 A. F. Demirörs, S. Aykut, S. Ganzeboom, Y. A. Meier and E. Poloni, Programmable droplet manipulation and wetting with soft magnetic carpets, *Proc. Natl. Acad. Sci. U. S. A.*, 2021, **118**(46), DOI: 10.1073/pnas.2111291118.

30 B. Peng, J. Xu, M. Fan, Y. Guo, Y. Ma, M. Zhou and Y. Fang, Smartphone colorimetric determination of hydrogen peroxide in real samples based on B, N, and S co-doped carbon dots probe, *Anal. Bioanal. Chem.*, 2020, **412**, 861–870, DOI: 10.1007/s00216-019-02284-1.

31 K.-J. Huang, D.-J. Niu, W.-Z. Xie and W. Wang, A disposable electrochemical immunosensor for carcinoembryonic antigen based on nano-Au/multi-walled carbon nanotubes–chitosans nanocomposite film modified glassy carbon electrode, *Anal. Chim. Acta*, 2010, **659**, 102–108, DOI: 10.1016/j.aca.2009.11.023.

32 C. Guo, F. Su, Y. Song, B. Hu, M. Wang, L. He, D. Peng and Z. Zhang, Aptamer-Templated Silver Nanoclusters Embedded in Zirconium Metal–Organic Framework for Bifunctional Electrochemical and SPR Aptasensors toward Carcinoembryonic Antigen, *ACS Appl. Mater. Interfaces*, 2017, **9**, 41188–41199, DOI: 10.1021/acsami.7b14952.

33 C.-H. Yeh, K.-F. Su and Y.-C. Lin, Development of an impedimetric immunobiosensor for measurement of carcinoembryonic antigen, *Sens. Actuators, A*, 2016, **241**, 203–211, DOI: 10.1016/j.sna.2016.01.053.

34 W. Lu, K. Wang, K. Xiao, W. Qin, Y. Hou, H. Xu, X. Yan, Y. Chen, D. Cui and J. He, Dual Immunomagnetic Nanobeads-Based Lateral Flow Test Strip for Simultaneous Quantitative Detection of Carcinoembryonic Antigen and Neuron Specific Enolase, *Sci. Rep.*, 2017, **7**, 42414, DOI: 10.1038/srep42414.

35 J. Yang, X. Xiao, L. Xia, G. Li and L. Shui, Microfluidic Magnetic Analyte Delivery Technique for Separation, Enrichment, and Fluorescence Detection of Ultratrace Biomarkers, *Anal. Chem.*, 2021, **93**, 8273–8280, DOI: 10.1021/acs.analchem.1c01130.